Dynamic Modeling of the Morphology of Latex Particles with *In Situ* Formation of Graft Copolymer

Elena Akhmatskaya,[1] José M. Asua[2]

[1]Basque Center for Applied Mathematics (BCAM), Building 500, Bizkaia Technology Park, E-48160, Derio, Spain
[2]Institute for Polymer Materials, POLYMAT, and Grupo de Ingeniería Química, Departamento de Química Aplicada, Facultad de Ciencias Químicas, University of the Basque Country, UPV/EHU, Joxe Mari Korta zentroa, Tolosa etorbidea 72, Donostia-San Sebastián 20018, Spain
Correspondence to: J. M. Asua (E-mail: jmasua@ehu.es)

Received 27 September 2011; accepted 12 December 2011; published online 12 January 2012
DOI: 10.1002/pola.25904

ABSTRACT: Modification of the polymer–polymer interfacial tension is a way to tailor-make particle morphology of waterborne polymer–polymer hybrids. This allows achieving a broader spectrum of application properties and maximizing the synergy of the positive properties of both polymers, avoiding their drawbacks. *In situ* formation of graft copolymer during polymerization is an efficient way to modify the polymer–polymer interfacial tension. Currently, no dynamic model is available for polymer–polymer hybrids in which a graft copolymer is generated during polymerization. In this article, a novel model based on stochastic dynamics is developed for predicting the dynamics of the development of particle morphology for composite waterborne systems in which a graft copolymer is produced *in situ* during the process. © 2012 Wiley Periodicals, Inc. J Polym Sci Part A: Polym Chem 50: 1383–1393, 2012

KEYWORDS: dynamic modeling; development of particle morphology; emulsion polymerization; grafting; graft copolymers; miniemulsion polymerization; morphology; polymer–polymer hybrid; seeded emulsion polymerization

INTRODUCTION The production of composite latex particles with well-defined morphology is a problem of great technical interest as they have a broader spectrum of properties than particles having uniform composition for applications such as coatings, adhesives, impact modifiers, and many other materials.[1–3] Composite latex particles are commonly prepared by seeded semicontinuous emulsion polymerization. A preformed latex (Polymer 1) is swollen with a certain amount of Monomer 2, and polymerization is started by adding initiator. Polymerization leads to the formation of chains of Polymer 2 in a matrix of Polymer 1 swollen with Monomer 2. Because of the incompatibility between the two polymers, phase separation occurs and clusters of Polymer 2 are formed within the matrix of Polymer 1. Polymerization continues in both clusters and matrix, and hence the clusters grow in size and new clusters are formed, which migrate toward the equilibrium morphology.[4–8] Depending on the polymerization conditions, a wide variety of particle morphologies can be produced: core shell,[9] "inverted" core shell,[10] hemispheres,[11] "raspberry-like,"[12] and void particles.[13]

Particle morphology depends on the interplay between thermodynamics and kinetics.[4–8,14,15] Thermodynamics determines the particle morphology at equilibrium, according to the minimum surface energy. Kinetic factors control whether the particle reaches the equilibrium morphology or remains at a metastable (kinetically stable) morphology.

The polymer–polymer and polymer–aqueous phase interfacial tensions play a key role in the development of the particle morphology as they determine the surface energy, and hence the equilibrium morphology. In addition, they strongly affect cluster migration toward the equilibrium morphology, that is, the kinetics.[4–6]

Modification of the polymer–polymer interfacial tension is a way to tailor-make particle morphology.[16–19] Thus, Rajatapiti et al.[16] prepared a miniemulsion of butyl acrylate containing a methyl methacrylate macromonomer, which upon polymerization led to the formation of the polybutyl acrylate seed with poly(butyl acrylate)–graft–poly(methyl methacrylate) copolymers. Polymerization of methyl methacrylate on this seed led to composite PBA/PMMA particles. The authors showed that morphology was strongly affected by the presence of the graft copolymer, which reduced the poly(butyl acrylate)–poly(methyl methacrylate) interfacial tension. For polystyrene–poly(methyl methacrylate) and polystyrene–poly(butyl acrylate), Herrera et al.[17–19] showed that block copolymers produced in situ by controlled radical polymerization (CRP) substantially modified the particle morphology.

The strategy consisted in adding during the formation of the seed a small amount of a CRP agent, so that some of the polymer chains were capped with the CRP agent at the end of the seed formation. Polymerization of the second-stage monomer in the presence of additional initiator led to the formation of some block copolymer chains that help to improve the compatibility of the two polymers. The practical importance of improving polymer–polymer compatibility is evident in the case of waterborne polymer–polymer hybrids (e.g., alkyd–acrylic,[20–22] polyurethane–acrylic,[23] and epoxy–acrylic[24]) that have been developed in an attempt to combine the positive properties of both polymers, avoiding their drawbacks.

Because of its scientific challenge and practical importance, modeling of the particle morphology has received considerable attention in literature. An excellent review[7] is available, which shows that the work is mainly restricted to the thermodynamic equilibrium morphology of two-phase systems. A model for the prediction of equilibrium morphologies of multiphase waterborne systems, such as polymer–polymer and polymer–polymer-inorganic hybrids has been recently developed.[25,26]

A large number of processes are carried out under conditions in which nonequilibrium morphologies are obtained.[8,27–32] These morphologies are governed by kinetics. González-Ortíz and Asua developed a model for the morphology development under dynamics conditions for two-phase systems.[4–6] However, no dynamic model is available for polymer–polymer hybrids in which a graft copolymer is generated *in situ* during polymerization.

In this article, a novel model based on stochastic dynamics is developed for predicting of the dynamics of the development of particle morphology for composite waterborne systems in which a graft copolymer is produced *in situ* during the process.

MATHEMATICAL MODEL

Polymer–polymer hybrid particles are commonly synthesized by seeded emulsion polymerization and miniemulsion polymerization. In the first case, the seed is produced by emulsion polymerization and then swollen with a second monomer or mixture of monomers. Polymerization of the second-stage monomer leads to the formation of the hybrid particle. Miniemulsion polymerization[33] is used when the first-stage polymer cannot be produced by emulsion polymerization because either it is too hydrophobic or it is produced by a method different from free radical polymerization such as step-growth polymerization.[34] In this case, the preformed polymer is dissolved in the monomer or mixture of monomers, miniemulsified using an adequate homogenization device[35,36] and the resulting miniemulsion is polymerized trying the nucleate most of the miniemulsion droplets and avoiding nucleation of particles by homogeneous nucleation. In both cases, the initial state of the second-stage polymerization is basically the same: a monomer swollen polymer particle, which is the system simulated in this work.

The preformed polymer will be referred to as Polymer 1. The monomer and the polymer resulting from its polymerization will be referred to as Monomer 2 and Polymer 2. In addition, some graft copolymer is formed during the polymerization that will be referred as graft.

A 200-nm particle with a composition polymer/monomer = 50/50 wt/wt is composed by about 1500 polymer chains (assuming a molecular weight of 750,000 g/mol, which is very common in polymerization in dispersed media) and about 11×10^6 molecules of monomer. Obviously, there is no way in which such a number of monomer molecules can be treated independently. Therefore, we pooled them in packs (subparticles) in such a way that polymerization of the monomer molecules contained in one subparticle led to one polymer chain. On the other hand, we treated the polymer chains individually (as subparticles). Assuming a density $\rho = 1$ kg/L for both polymer and monomer, the diameter of each subparticle would be $\sigma = 13.3$ nm. The water surrounding the particle was also pooled in subparticles. For simplicity, the water subparticles were considered to have the same size as the monomer and polymer spheres. In the model, each subparticle was represented by a sphere that interacts with its neighbors.

In the simulations, the system at the beginning of the process was considered to be formed by Polymer 1 (1564 subparticles) and Monomer 2 (1564 subparticles) surrounded by water (4340 subparticles). A spherical simulation cell of diameter 32σ was used to fit the 7458 subparticles of size σ.

The nonbonded interactions between two subparticles i and j of Polymer 1–Polymer 1; Polymer 2–Polymer 2; Monomer 2–Monomer 2; graft–graft; graft–Polymer 1; graft–Polymer 2; and water–water as well as the interaction between Polymer 1–Monomer 2; Polymer 2–Monomer 2; and graft–Monomer 2 with relative positions $r_i - r_j = r_{ij}\hat{r}_{ij}$ (the hat indicating a unit vector) were modeled by the Lennard–Jones potential,

$$U_{\mathrm{LJ}}(r_{ij}) = 4\varepsilon\left[\left(\frac{\sigma}{r_{ij}}\right)^{12} - \left(\frac{\sigma}{r_{ij}}\right)^{6}\right] \quad (1)$$

where ε is the depth of the potential well.

A repulsive generalized soft sphere potential was used for the interactions between dissimilar phases: Polymer 1–Polymer 2; Polymer 1–water; Polymer 2–water; graft–water; and Monomer 2–water

$$U_r(r_{ij}) = \varepsilon\left(\frac{\sigma}{r_{ij}}\right)^{6}. \quad (2)$$

To keep the polymer and monomer subparticles within the particle and to reproduce a continuous aqueous phase out of the sphere; we introduced an impenetrable structureless wall of the simulation sphere. Therefore, for Polymer 1, Monomer 2, Polymer 2, and graft subparticles, a repulsive generalized soft sphere potential was used to prevent them

from moving from the center of the simulation further than a distance R_c:

$$U_{\text{poly-wall}}(r_{ij}) = \begin{cases} \varepsilon\left(\frac{\sigma}{R_c - r_{ij}}\right)^6 & \text{for } r_{ij} > R_c - 2^{1/6}\sigma \\ 0 & \text{for } r_{ij} \leq R_c - 2^{1/6}\sigma \end{cases} \quad (3)$$

To monitor the distances between subparticles and the wall, a dummy, frozen particle was placed in a center of the simulation cell and used to determine the distances between the particles and the wall as a difference between the radius of the simulation cell and the distance between the particles and the dummy frozen particle.

The interactions between water spheres and the wall of the simulation cell were also described using water–frozen dummy particle interactions, which in this case were chosen to be Lennard–Jones potentials:

$$U_{\text{water-wall}}(r_{ij}) = \begin{cases} U_{\text{LJ}}(R_c - r_{ij}) & \text{for } r_{ij} > R_c - 2.5\sigma \\ 0 & \text{for } r_{ij} \leq R_c - 2.5\sigma \end{cases} \quad (4)$$

In eqs 3 and 4, r_{ij} is the distance between the subparticles and the center of the simulation sphere (the frozen dummy particle) and

$$R_c = \begin{cases} 16 & \text{for water particles} \\ 13 & \text{for monomer and polymer particles} \end{cases} \quad (5)$$

The simulation included two steps. First, the structure of the initial monomer swollen polymer particle was calculated. Second, the dynamics of the particle morphology development caused by polymerization of Monomer 2 and graft formation was simulated.

In the simulations, it was considered that Monomer 2 and Polymer 1 were compatible. To determine the structure of the monomer swollen initial particle, a preliminary distribution of Polymer 1, Monomer 2, and water subparticles was chosen and then the system was equilibrated using stochastic dynamics simulation.

The preliminary distribution of Polymer 1, Monomer 2, and water subparticles was chosen as follows. First, the subparticles representing the Polymer 1, Monomer 2, and water were positioned randomly within a simulation sphere of a diameter equal to 32σ, closer to the center. The simulation sphere was surrounded by a layer of vacuum of 2.5σ. To form the proper minimized starting configuration for the equilibrating stochastic dynamics run, the steepest descent method with a dimensionless maximum step size of 0.001 and a tolerance of 10 was performed for 4000 minimization steps for the randomly set system. The initial structure of the monomer swollen polymer particle immersed in water was then determined by running the stochastic dynamics simulation for $t = 2000$.

A problem associated to the random distribution of subparticles is that the density of subparticles achieved by means of the initial random placement of subparticles in the simulation cell is lower than that at equilibrium. Therefore, rearrangement of the subparticles during the minimization of the energy of the system leads to the formation of vacuum regions that disturbs the calculation of the energy of the system, because the subparticles at the borders of the vacuum regions are not subjected to interactions with other subparticles. This leads to unrealistic structures. To avoid this problem, first the subparticles were randomly distributed using the values of R_c given in eq 5 and the system was equilibrated for $t = 2000$. Then, the values of R_c were modified to $R_c = 15.7$ for water particles and $R_c = 12.5$ for Polymer 1 and Monomer 2 subparticles and the system was equilibrated again for $t = 2000$. This gave the starting configuration for the calculation of the development of the particle morphology during polymerization using stochastic dynamics simulation.

The dynamics of the particle morphology development was simulated by means of the velocity Langevin dynamics performed in the NVT ensemble:

$$m\frac{d^2r}{dt^2} = \nabla U - \gamma m\frac{dr}{dt} + \sqrt{2\gamma k_B T m}R(t) \quad (6)$$

where

$$< R(t) >= 0; < R(t)R(t') >= \delta(t - t'). \quad (7)$$

A dimensionless Langevin equation was obtained by using $x = r/\sigma$; $\varepsilon^* = \varepsilon/\varepsilon'$; $U^* = U/\varepsilon'$; and $t^* = t/\tau$ where $\tau = \sqrt{m\sigma^2/\varepsilon'}$ and ε' is a reference potential that in this work was taken as 4.74×10^{-21} J.

$$\frac{d^2x}{dt^{*2}} = \nabla U^* - \frac{\gamma}{\left(\frac{\varepsilon'}{m\sigma^2}\right)^{0.5}}\frac{dx}{dt^*} + \sqrt{2\frac{\gamma}{\left(\frac{\varepsilon'}{m\sigma^2}\right)^{0.5}}\frac{k_B T}{\varepsilon'}\frac{R^2(t)}{\left(\frac{\varepsilon'}{m\sigma^2}\right)^{0.5}}} \quad (8)$$

One of the challenges during the second stage of the synthesis of complex waterborne particles is to avoid secondary nucleation (formation of new particles by homogeneous nucleation), because the new particles formed will only contain Polymer 2. Homogeneous nucleation is enhanced when water-soluble initiators are used. Therefore, oil-soluble initiators are often used and they were simulated in this work.

Polymerization of Monomer 2 to produce Polymer 2 was simulated by converting the monomer subparticles into subparticles of a new polymeric phase (Polymer 2). In addition, grafting was simulated by converting Monomer 2 and Polymer 1 subparticles into graft subparticles. The extent of grafting was controlled by the ratio of Monomer 2 subparticles giving Polymer 2 and those giving graft copolymer. In addition, the composition of the graft copolymer was controlled by the ratio between the Monomer 2 and Polymer 1 subparticles involved in the grafting reaction. In these processes, new types of subparticles appeared in the system, but the total number of simulated subparticles was constant during the simulation process. For the examples presented in this article, it was considered that a fraction of Monomer 2 (either 60% or 80%) became Polymer 2 and the rest of

Monomer 2 (either 40% or 20%) reacted on Polymer 1 to give a graft copolymer of 50/50 (Polymer 1/Polymer 2) composition. In addition, the initial Monomer 2/Polymer 1 composition was 50/50.

To simulate the polymerization, the subparticles of Monomer 2 that led to Polymer 2 (either 60% or 80% of the total) as well as those of Monomer 2 and Polymer 1 that underwent grafting reactions were randomly chosen. These groups were called GP2, GG2, and GG1, respectively. Unless otherwise stated, the kinetics was simulated by considering that the conversion of Monomer 2 into Polymer 2 and graft copolymer occurred in M steps. In each of M steps, $1/M$th subparticles were randomly chosen from each group, GP2, GG2, and GG1 and gradually converted into Polymer 2 and graft copolymer over a certain process period. A constant polymerization rate, which represents well what has been reported for miniemulsion polymerization using oil-soluble initiators,[37] was used, namely, the same time was allocated to each of the M steps. The transformation of the monomer (and Polymer 1 in the grafting reactions) into the new polymers (Polymer 2 and graft copolymer) was achieved by gradually changing the interactions from those of the monomer (and Polymer 1) to the characteristic values of the new polymers. Thus, when Monomer 2 is converted to Polymer 2, the Lennard–Jones interaction for Monomer 2–Polymer 1 was replaced by a repulsive potential for Polymer 1–Polymer 2. The random choice of the monomer subparticles implies that a uniform distribution of radicals within the polymer particles was assumed, which is consistent with the use of oil-soluble initiators

If water-soluble initiators are used, the distribution of radicals may not be uniform because of the anchoring effect of the hydrophilic part of the entering radical to the surface of the particle. However, this is not always the case. Thus, noncharged water-soluble initiators (e.g., *t*-butyl hydroperoxide) and monomers with a high chain transfer to monomer (e.g., vinyl acetate) lead to much more homogeneous radical concentrations.

To apply the present model to cases in which a profile of radical concentration in the particle exist, the distribution of radicals in the particle may be calculated using the available methods[38,39] and the monomer subparticles that are going to undergo polymerization in a given time interval are chosen according to the radical concentration profile, namely giving a higher probability of reaction to the monomer subparticles that are near the surface of the particle.

The friction factor (γ) controls the rate at which the phases move in the particle and it increases with the internal viscosity of the particle. High values of γ correspond to high internal viscosity of the particle. This leads to a slow phase migration and for fast polymerization rates, it may result in a system in which Polymer 2 remains in the place where it is formed. On the other hand, low values of γ correspond to low particle viscosity that may lead to equilibrium morphologies. In addition, as the viscosity increases as $\eta \div \phi^5$ (ϕ being the volume fraction of polymer[40]), in some of the simulations presented in this work, the following equation was used for the friction factor

$$\gamma = \gamma_0(0.5 + 0.5x)^5 \tag{9}$$

where x is the conversion of monomer and γ_0 is the value of γ at $x = 1$. The actual value of γ_0 depends on the particular system considered, and for the sake of the simulations performed in this work, the value of γ_0 was estimated by considering that it is related to the diffusion coefficient (D) as

$$\gamma_0 = \frac{k_B T}{mD} \tag{10}$$

Polymer diffusion has been extensively investigated during film formation from latexes and the diffusion coefficients have been estimated using fluorescence resonance energy transfer (FRET) methods.[41–44] In these works it can be seen that the value of D depends on both the system considered and the temperature of the experiment, but for $T = 70$ °C, a value of $D = 5 \times 10^{-18}$ m^2 s^{-1} is reasonable, which gives a value of $\gamma_0 = 7.6 \times 10^{17}$ s^{-1}.

All simulations were performed using the GROMACS 4.0.7 code[45] in parallel on the computing cluster comprising 29 computing elements composed by 2 Intel QuadCore Xeon processors. The visualization molecular dynamics tool, VMD,[46] has been used for analysis of the SD trajectories and for creating figures for this article. In GROMACS, the accuracy of the integration of the dimensionless Langevin equation decreases with the increasing product $\gamma \times \tau \times \Delta t^*$, where Δt^* is the time increment in the integration. As a reference, a $\Delta t^* = 0.005$ should often be used to integrate the dimensionless Langevin equation with a reasonable accuracy. Therefore, the corresponding real time, Δt, which is equal to $\tau \times \Delta t^*$, is very small (about 3×10^{-11} s with the values of the parameters discussed above). This means that to simulate a polymerization of 1 h, 1.2×10^{14} integration steps are needed, which results in an unaffordable computer time (the maximum affordable number of integration steps is estimated to be about 1.5×10^7).

A solution to this problem can be found considering the migration of phases in a particle containing Polymer 1, Polymer 2, and Monomer 2, and in which no polymerization occurs. The movement of the phase i can be described by means of a classical material balance

$$\frac{\partial c_i}{\partial t} = -\nabla \cdot D \nabla C_i \tag{11}$$

where D is an effective diffusion coefficient that includes both Brownian and the interaction terms and C_i is the concentration of phase i (Polymer 1, Polymer 2, and Monomer 2).

Equation 11 is interesting because if due to computation limitations it is not possible to integrate eq 11 for longer than a certain time, for example, 1 s, it is still possible to obtain the evolution of the concentration of phase i that in the real

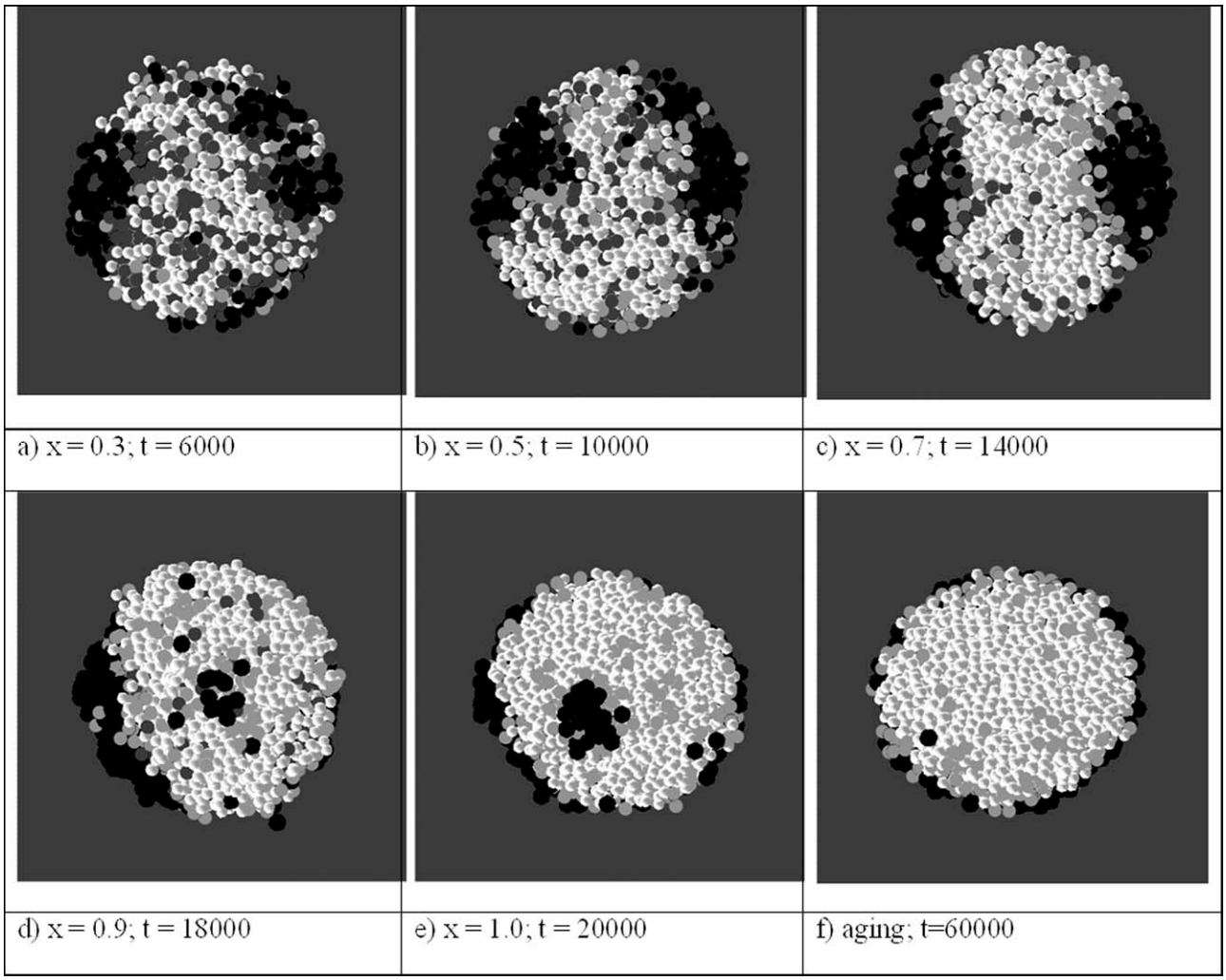

FIGURE 1 Particle morphology evolution in Run 1 (20% of graft copolymer). The ε^* values are given in Table 1. Legend: Polymer 1 (white); Monomer 2 (dark gray); Polymer 2 (black); graft (light gray); x is the conversion rate; t is the time in reduced units.

system occurs over a longer time scale, for example, 10^4 s, by simply using a value of the effective diffusion coefficient equal to $D \times 10^4$. In the framework of the Langevin equation, the effective diffusion coefficient is inversely proportional to γ, therefore, if a Langevin equation is used to describe this example, it would be sufficient to use a value of γ equal to $\gamma \times 10^{-4}$.

For a polymerizing system, the material balance becomes:

$$\frac{\partial C_i}{\partial t} = -\nabla \cdot D\nabla C_i + R_i \tag{12}$$

where R_i is the rate of generation of phase i (in the case of consumption it appears with a negative sign). From eq 12, it

TABLE 1 Values of ε^* Used in Runs 1, 6, and 7

	Polymer 1	Monomer 2	Polymer 2	Graft	Water	Wall
Polymer 1	$\varepsilon_{P1-P1} = 1.3$	$\varepsilon_{P1-M2} = 1.3$	$\varepsilon_{P1-P2} = 0.6$	$\varepsilon_{P1-graft} = 1$	$\varepsilon_{P1-W} = 6$	$\varepsilon_{P1-wall} = 6$
Monomer 2	$\varepsilon_{M2-P1} = 1.3$	$\varepsilon_{M2-M2} = 1.3$	$\varepsilon_{M2-P2} = 1.3$	$\varepsilon_{M2-graft} = 1.3$	$\varepsilon_{M2-W} = 6$	$\varepsilon_{M2-wall} = 6$
Polymer 2	$\varepsilon_{P2-P1} = 0.6$	$\varepsilon_{P2-M2} = 1.3$	$\varepsilon_{P2-P2} = 1.3$	$\varepsilon_{P2-graft} = 1$	$\varepsilon_{P2-W} = 2$	$\varepsilon_{P2-wall} = 6$
Graft	$\varepsilon_{graft-P1} = 1$	$\varepsilon_{graft-M2} = 1.3$	$\varepsilon_{graft-P2} = 1$	$\varepsilon_{graft-graft} = 1.3$	$\varepsilon_{graft-W} = 4$	$\varepsilon_{graft-wall} = 6$
Water	$\varepsilon_{W-P1} = 6$	$\varepsilon_{W-M2} = 6$	$\varepsilon_{W-P2} = 2$	$\varepsilon_{W-graft} = 4$	$\varepsilon_{W-W} = 1$	$\varepsilon_{W-wall} = 1$
Wall	$\varepsilon_{wall-P1} = 6$	$\varepsilon_{wall-M2} = 6$	$\varepsilon_{wall-P2} = 6$	$\varepsilon_{wall-graft} = 6$	$\varepsilon_{wall-W} = 1$	

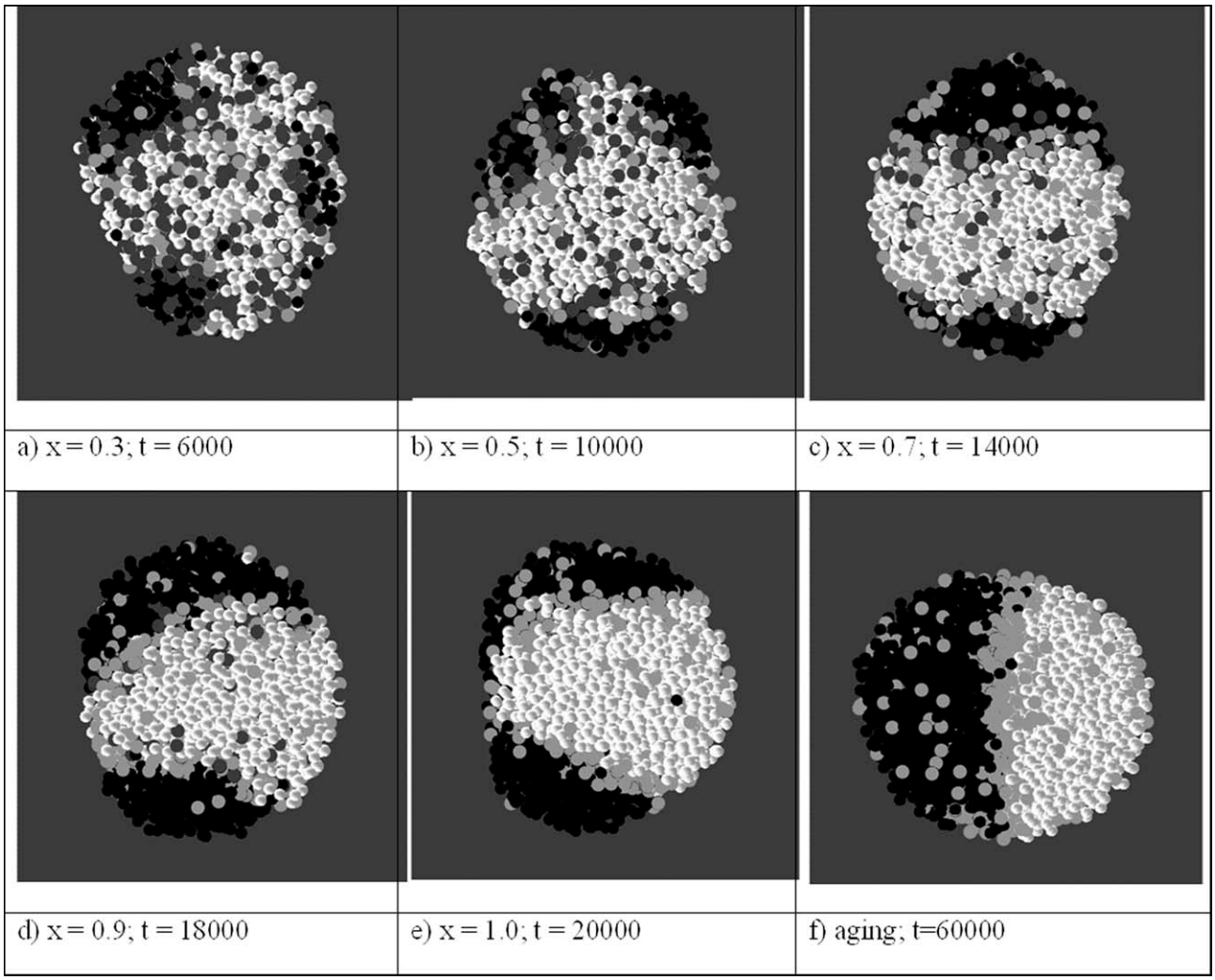

FIGURE 2 Particle morphology evolution in Run 2 (20% of graft copolymer). The ε^* values are given in Table 2. Legend: Polymer 1 (white); Monomer 2 (dark gray); Polymer 2 (black); graft (light gray); *x* is the conversion rate; t is the time in reduced units.

is evident that to simulate the system over a longer time scale, the rate of generation of phase *i* should also be multiplied for the same factor than *D*.

Therefore, to simulate a 1 h process using the Langevin equation with a maximum of 1.5×10^7 integration steps and a real time increment of 3×10^{-11} s, the value of γ_0 to be used in the simulation is $\gamma_0/(8 \times 10^6)$.

REPRESENTATIVE SIMULATIONS

Figure 1 presents the evolution of the particle morphology in a system in which Polymer 1 was more hydrophobic than Polymer 2 and 20% of the converted Monomer 2 was incorporated into the graft copolymer, which had a composition Polymer 1/Polymer 2 = 50/50. Therefore, at complete conversion, graft copolymer represented 20% of the total

TABLE 2 Values of ε^* Used in Runs 2 and 3

	Polymer 1	Monomer 2	Polymer 2	Graft	Water	Wall
Polymer 1	$\varepsilon_{P1-P1} = 1.3$	$\varepsilon_{P1-M2} = 1.3$	$\varepsilon_{P1-P2} = 0.6$	$\varepsilon_{P1-graft} = 1$	$\varepsilon_{P1-W} = 6$	$\varepsilon_{P1-wall} = 6$
Monomer 2	$\varepsilon_{M2-P1} = 1.3$	$\varepsilon_{M2-M2} = 1.3$	$\varepsilon_{M2-P2} = 1.3$	$\varepsilon_{M2-graft} = 1.3$	$\varepsilon_{M2-W} = 6$	$\varepsilon_{M2-wall} = 6$
Polymer 2	$\varepsilon_{P2-P1} = 0.6$	$\varepsilon_{P2-M2} = 1.3$	$\varepsilon_{P2-P2} = 1.3$	$\varepsilon_{P2-graft} = 1$	$\varepsilon_{P2-W} = 6$	$\varepsilon_{P2-wall} = 6$
Graft	$\varepsilon_{graft-P1} = 1$	$\varepsilon_{graft-M2} = 1.3$	$\varepsilon_{graft-P2} = 1$	$\varepsilon_{graft-graft} = 1$	$\varepsilon_{graft-W} = 6$	$\varepsilon_{graft-wall} = 6$
Water	$\varepsilon_{W-P1} = 6$	$\varepsilon_{W-M2} = 6$	$\varepsilon_{W-P2} = 6$	$\varepsilon_{W-graft} = 6$	$\varepsilon_{W-W} = 1$	$\varepsilon_{W-wall} = 1$
Wall	$\varepsilon_{wall-P1} = 6$	$\varepsilon_{wall-M2} = 6$	$\varepsilon_{wall-P2} = 6$	$\varepsilon_{wall-graft} = 6$	$\varepsilon_{wall-W} = 1$	

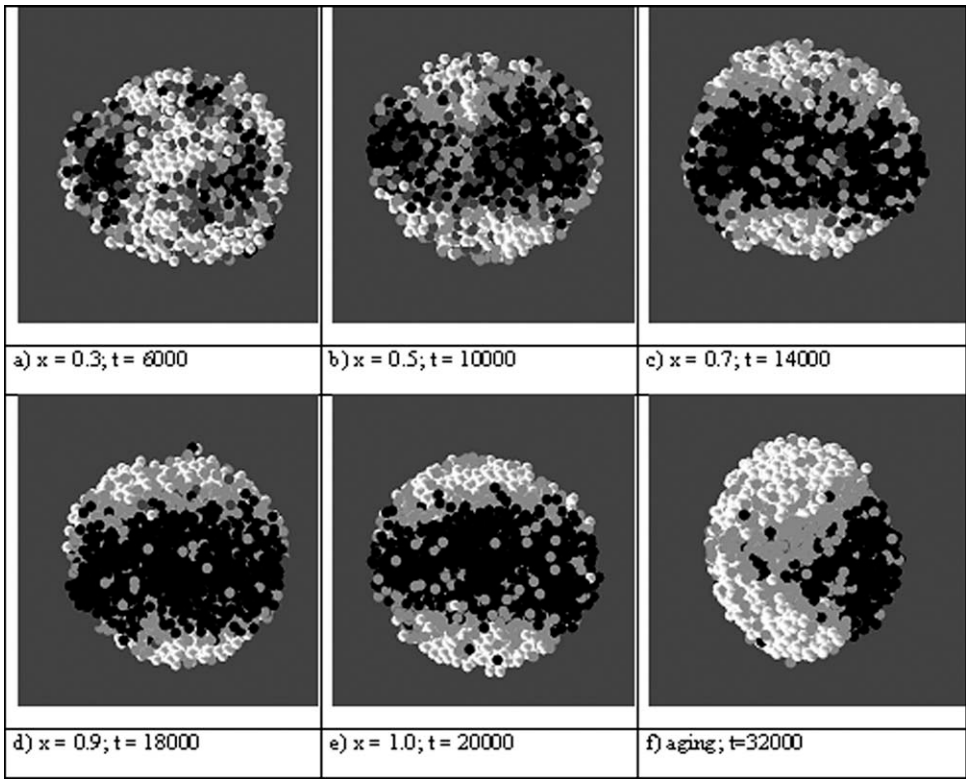

FIGURE 3 Particle morphology evolution in Run 3 (40% of graft copolymer). The ε^* values are given in Table 2. Legend: Polymer 1 (white); Monomer 2 (dark gray); Polymer 2 (black); graft (light gray); *x* is the conversion rate; t is the time in reduced units.

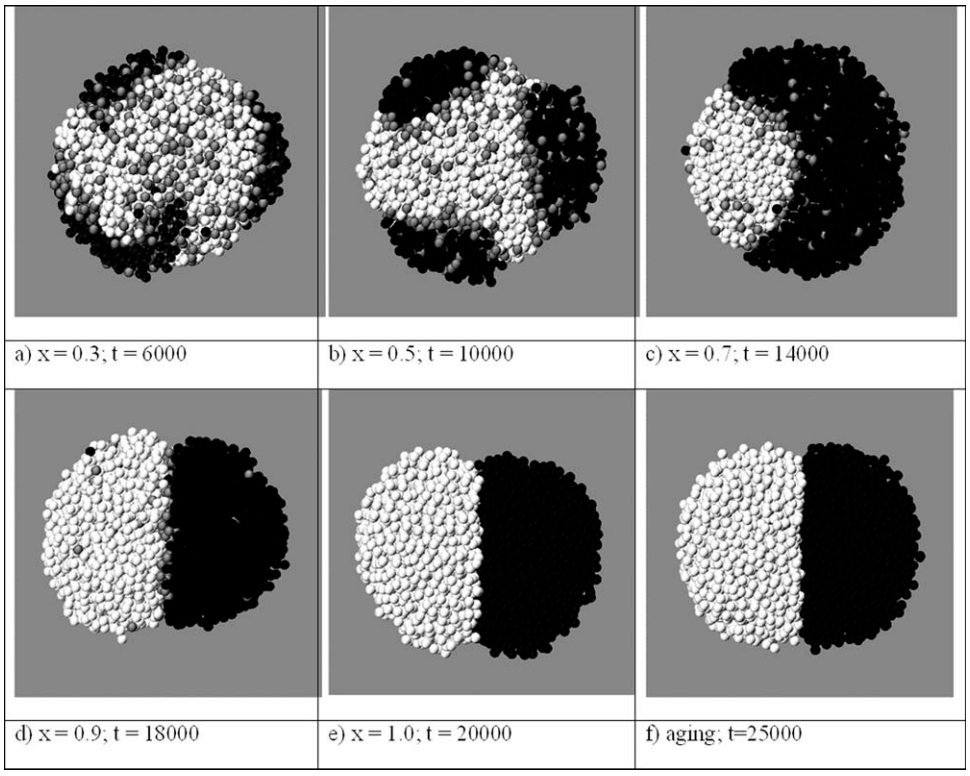

FIGURE 4 Particle morphology evolution in Run 4, in which no graft copolymer was formed. The ε^* values are given in Table 3. Legend: Polymer 1 (white); Monomer 2 (gray); Polymer 2 (black); *x* is the conversion rate; t is the time in reduced units.

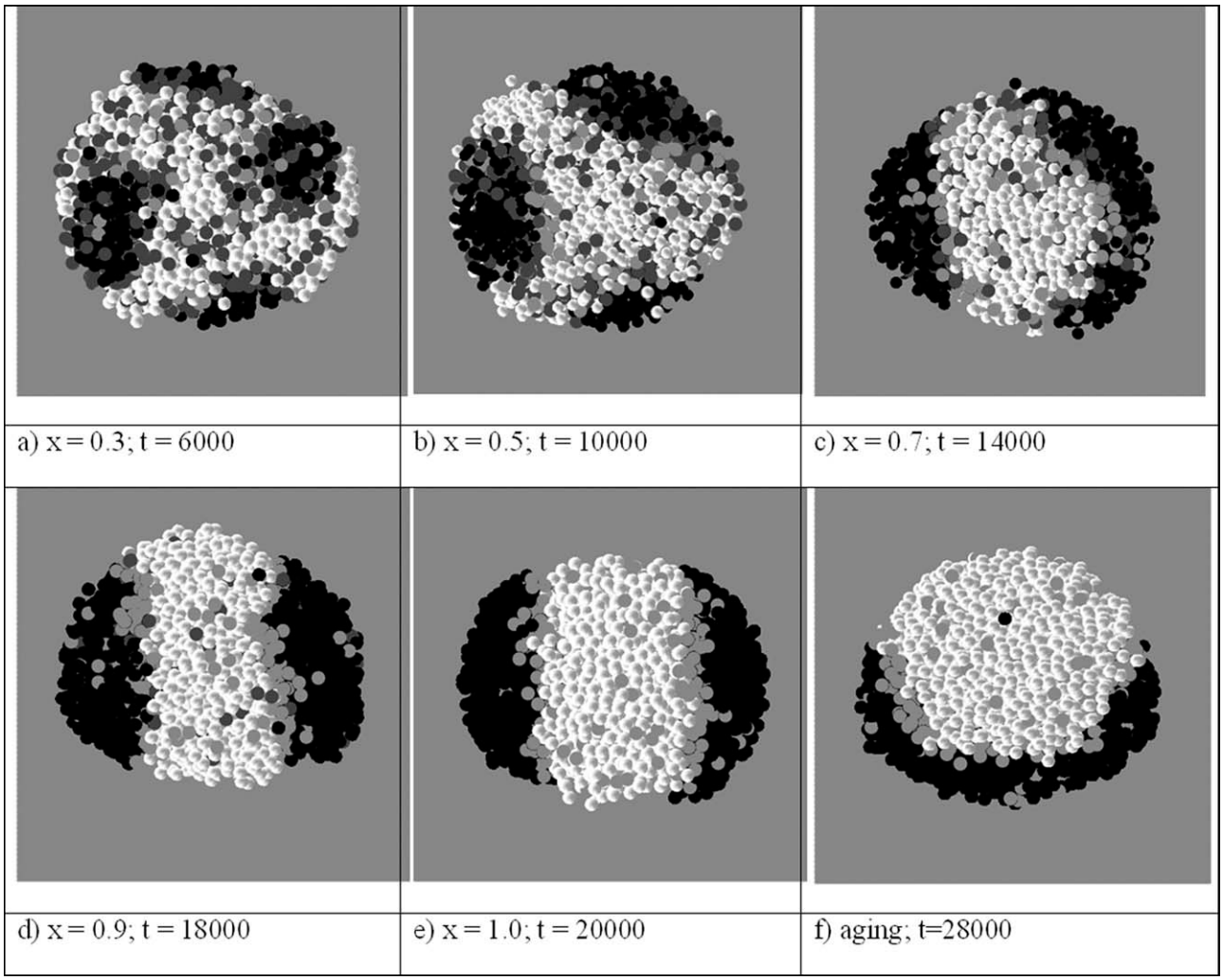

FIGURE 5 Particle morphology evolution in Run 5 (20% of graft copolymer). The ε^* values are given in Table 3. Legend: Polymer 1 (white); Monomer 2 (dark gray); Polymer 2 (black); graft (light gray); *x* is the conversion rate; t is the time in reduced units.

polymer. The parameters used in the simulation are given in Table 1. A constant dimensionless friction factor $\gamma/(\varepsilon'/m\sigma^2)^{0.5} = 20$ was used in this simulation. Figure 1 shows that Polymer 2 (black) migrated toward the outer part of the particle whereas Polymer 1 (white) moved toward the interior of the particle and the graft copolymer (light gray) was placed between Polymers 1 and 2. For the conditions used in the simulation of Run 1, a nonequilibrium morphology was obtained when complete conversion of Monomer 2 was reached [Fig. 1(e)]. Inverted core-shell equilibrium morphology was achieved upon aging [Fig. 1(f)].

Figure 2 presents the evolution of the particle morphology in a system in which Polymers 1 and 2 were similarly hydrophobic (Run 2). The polymerization rate and the amount and composition of the graft copolymer were the same as in Run 1. The values of ε^* used in the simulation are given in Table

TABLE 3 Values of ε^* Used in Runs 4 and 5

	Polymer 1	Monomer 2	Polymer 2	Graft	Water	Wall
Polymer 1	$\varepsilon_{P1-P1} = 1.3$	$\varepsilon_{P1-M2} = 1.3$	$\varepsilon_{P1-P2} = 1.5$	$\varepsilon_{P1-graft} = 1$	$\varepsilon_{P1-W} = 6$	$\varepsilon_{P1-wall} = 6$
Monomer 2	$\varepsilon_{M2-P1} = 1.3$	$\varepsilon_{M2-M2} = 1.3$	$\varepsilon_{M2-P2} = 1.3$	$\varepsilon_{M2-graft} = 1.3$	$\varepsilon_{M2-W} = 6$	$\varepsilon_{M2-wall} = 6$
Polymer 2	$\varepsilon_{P2-P1} = 1.5$	$\varepsilon_{P2-M2} = 1.3$	$\varepsilon_{P2-P2} = 1.3$	$\varepsilon_{P2-graft} = 1$	$\varepsilon_{P2-W} = 4$	$\varepsilon_{P2-wall} = 6$
Graft	$\varepsilon_{graft-P1} = 1$	$\varepsilon_{graft-M2} = 1.3$	$\varepsilon_{graft-P2} = 1$	$\varepsilon_{graft-graft} = 1.3$	$\varepsilon_{graft-W} = 5$	$\varepsilon_{graft-wall} = 6$
Water	$\varepsilon_{W-P1} = 6$	$\varepsilon_{W-M2} = 6$	$\varepsilon_{W-P2} = 4$	$\varepsilon_{W-graft} = 5$	$\varepsilon_{W-W} = 1$	$\varepsilon_{W-wall} = 1$
Wall	$\varepsilon_{wall-P1} = 6$	$\varepsilon_{wall-M2} = 6$	$\varepsilon_{wall-P2} = 6$	$\varepsilon_{wall-graft} = 6$	$\varepsilon_{wall-W} = 1$	

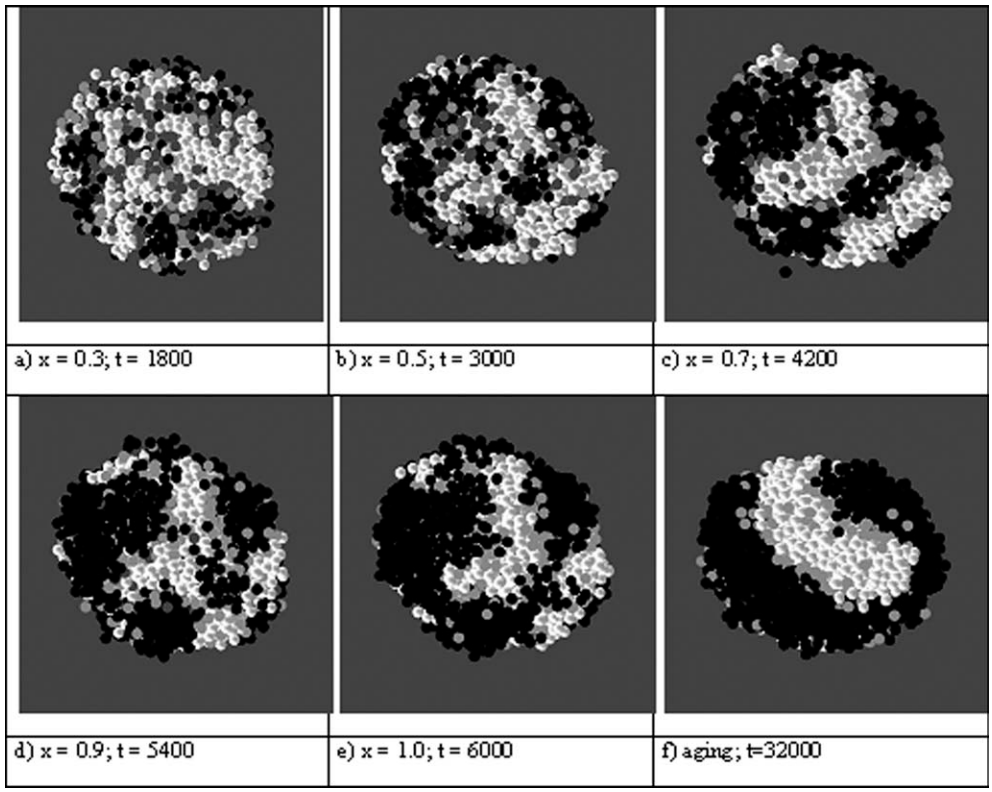

FIGURE 6 Particle morphology evolution in Run 6 (20% of graft copolymer). The ε^* values are given in Table 1. Legend: Polymer 1 (white); Monomer 2 (dark gray); Polymer 2 (black); graft (light gray); *x* is the conversion rate; t is the time in reduced units.

2. It can be seen that because of their similar hydrophobicity, Polymers 1 and 2 were in contact with water, whereas the graft copolymer was placed between them. At the end of the polymerization, a nonequilibrium morphology was reached [Fig. 2(e)] that upon aging led to a hemispherical equilibrium configuration.

Figure 3 presents the evolution of the particle morphology in a system (Run 3) in which Polymers 1 and 2 were the same as in Run 2, but the amount of graft copolymer was higher (40%). The polymerization rate was the same as in Run 2. Comparison with Figure 2 shows that the extent of grafting strongly affected the evolution of the particle morphology, the phase migration being slower for the case in which a higher amount of graft copolymer was produced.

Figures 4 and 5 show the effect of the formation of grafting on the evolution of the particle morphology. The parameters used are given in Table 3. In Run 4 (Fig. 4), it was considered that no graft polymer was formed; whereas in Run 5 (Fig. 5), 20% of graft copolymer was formed. In can be seen that in the absence of grafting, the particle morphology evolves toward a hemispherical morphology, whereas in the case in which graft copolymer was formed, the morphology approached core-shell morphology. This shows the potential of the modification of the polymer–polymer interfacial tension to tailor-make particle–particle morphology. The predictions closely reproduced the experimental results obtained by Herrera et al.[17,18] for polystyrene–poly(methyl methacrylate) producing block copolymers *in situ* by means of CRP.

In the simulations presented in Figures 1–5, a constant viscosity within the polymer particle was considered. However, the internal viscosity of the particle continuously increases during polymerization because of the conversion of Monomer 2. Figure 6 presents the evolution of the polymer particle (Run 6) considering the variation of the friction factor given by eq 9 and a faster polymerization rate for the parameters used in Run 1 (Table 1). Comparison between Figures 1 and 6 shows that the evolution of the particle morphology was retarded because of the combined effect of the increase of the internal viscosity of the particle and the faster polymerization rate.

Figure 7 presents the evolution of the particle morphology in a system similar to that of Run 6, but in which all the grafting occurred in a time of 3000 reduced units, whereas the polymerization of Monomer 2 to Polymer 2 required a time of 6000 reduced units. Comparison of this figure with Figure 6 illustrates the effect of the relative rates of grafting and polymerization showing that the early grafting retarded phase separation during the initial stages of the polymerization, but later they tend to the same equilibrium morphology, which is difficult to reach because of the high-internal viscosity of the final polymer particle.

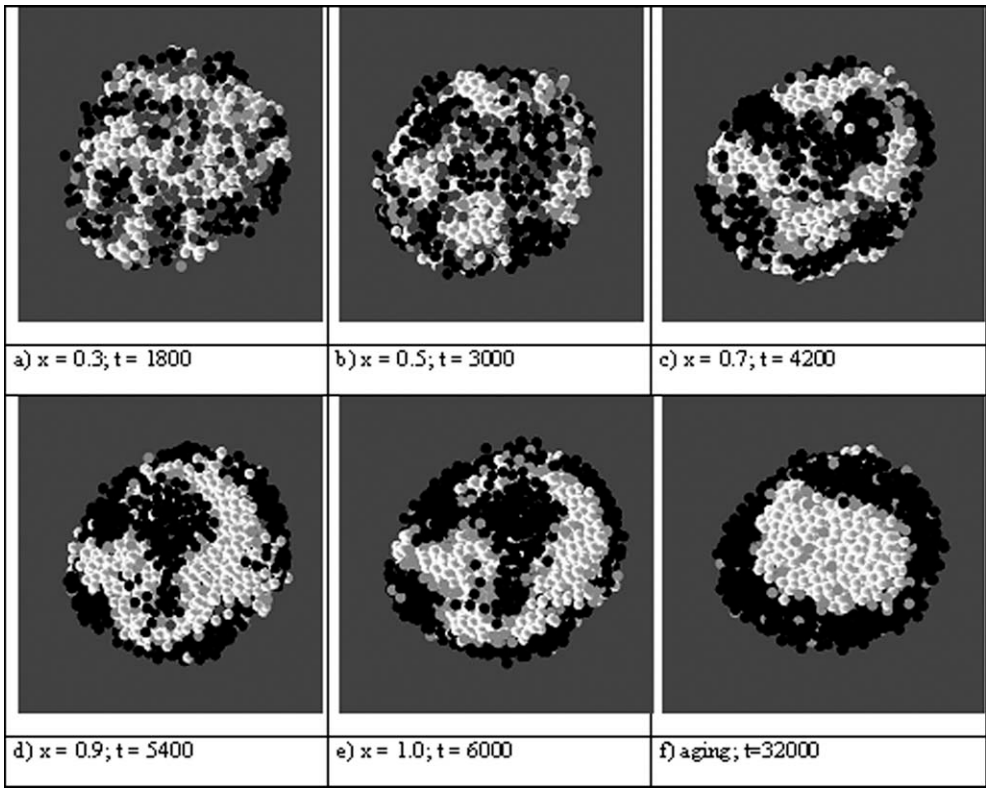

FIGURE 7 Particle morphology evolution in Run 7 (20% of graft copolymer). The ε^* values are given in Table 1. Legend: Polymer 1 (white); Monomer 2 (dark gray); Polymer 2 (black); graft (light gray); *x* is the conversion rate; t is the time in reduced units.

CONCLUSIONS

In this article, a novel model based on stochastic dynamics was developed for predicting the dynamics of the development of particle morphology of composite waterborne systems in which a graft copolymer is produced *in situ* during the process. The model accounts for the effects of phase compatibility and internal viscosity of the particles and is able to predict the effect of formation of grafting on particle morphology for which there was no method available. The predictions closely reproduced experimental results.

The authors thank the support of the computing infrastructure of the i2BASQUE academic network. The financial support from Diputacion Foral de Gipuzkoa, Basque Government (GV IT373-10 and SAIOTEK 2010 Ref. S-PE10UN25) and Ministerio de Ciencia y Tecnología (CTQ 2011-25572) are gratefully acknowledged.

REFERENCES AND NOTES

1 Polymeric Dispersions: Principles and Applications; Asua, J. M., Ed.; Kluwer Academic Publishers: Dordrecht, **1997**.

2 Emulsion Polymerization and Emulsion Polymers; Lovell, P. A.; El-Aasser, M. S., Eds.; Wiley: Chichester, **1997**.

3 Urban, D.; Takamura, K. Polymer Dispersions and their Industrial Applications. Wiley-VCH Verlag: Weinheim, **2002.**

4 González-Ortiz, L. J.; Asua, J. M. *Macromolecules* **1995,** *28*, 3135–3145.

5 González-Ortiz, L. J.; Asua, J. M. *Macromolecules* **1996,** *29*, 383–389.

6 González-Ortiz, L. J.; Asua, J. M. *Macromolecules* **1996,** *29*, 4520–4527.

7 Sundberg, D. C.; Durand, Y. G. *Polym. React. Eng.* **2003,** *11*, 379–432.

8 Chen, Y. C.; Dimonie, V. L.; El-Aasser, M. S. *J. Appl. Polym. Sci.* **1992,** *45*, 487–499.

9 Min, T. I.; Klein, A.; El-Aasser, M. S.; Vanderhoff, J. W. *J. Polym. Sci.: Polym. Chem. Ed.* **1983,** *21*, 2845–2861.

10 Lee, D. I.; Ishikawa, T. *J. Polym. Sci.: Polym. Chem. Ed.* **1983,** *21*, 147–154.

11 Sheu, H. R.; El-Aasser, M. S.; Wanderhoff, J. W. *J. Polym. Sci. Part A: Polym. Chem.* **1990,** *28*, 653–667.

12 Okubo, M.; Katsuta, Y.; Matsumoto, T. *J. Polym. Sci.: Polym. Lett. Ed.* **1980,** *18*, 481–486.

13 Okubo, M.; Nakagawa, T. *Colloid Polym. Sci.* **1994,** *272*, 45–51.

14 Sundberg, D. C.; Casassa, A. P.; Pautazopoulus, J.; Muscato, M. R.; Kronberg, B.; Berg, J. *J. Appl. Polym. Sci.* **1990,** *41*, 1425–1442.

15 Chen, Y. C.; Dimonie, V. L.; Shaffer, O.; El-Aasser, M. S. *Polym. Int.* **1993,** *30*, 185–194.

16 Rajatapiti, P.; Dimonie, V. L.; El-Aasser, M. S. *J. Macromol. Sci. Pure: Appl. Chem.* **1995,** *A32*, 1445–1460.

17 Herrera, V.; Pirri, R.; Leiza, J. R.; Asua, J. M. *Macromolecules* **2006,** *39*, 6969–6974.

18 Herrera, V.; Pirri, R.; Asua, J. M.; Leiza, J. R. *J. Polym. Sci. Part A: Polym. Chem.* **2007,** *45*, 2484–2493.

19 Herrera, V.; Pirri, R.; Leiza, J. R.; Asua, J. M. *Macromolecules* **2010,** *43*, 1356–1363.

20 Tsavalas, J. G.; Schork, F. J.; Landfester, K. J. *Coat. Technol.* **2004,** *1*, 53–63.

21 Goikoetxea, M.; Minari, R. J.; Beristain, I.; Paulis, M.; Barandiarán, M. J.; Asua, J. M. *J. Polym. Sci. Part A: Polym. Chem.* **2009,** *47*, 4871–4885.

22 Goikoetxea, M.; Minari, R. J.; Beristain, I.; Paulis, M.; Barandiaran, M. J.; Asua, J. M. *Polymer* **2010,** *51*, 5313–5317.

23 Li, C. Y.; Chiu, W. Y.; Don, T. M. *J. Polym. Sci. Part A: Polym. Chem.* **2007,** *45*, 3359–3369.

24 Kawahara, H.; Goto, T.; Ohnishi, K.; Ogura, H.; Kage, H.; Matsuno, Y. *J. Appl. Polym. Sci.* **2001,** *81*, 128–133.

25 Reyes, Y.; Asua, J. M. *J. Polym. Sci. Part A: Polym. Chem.* **2010,** *48*, 2579–2583.

26 Reyes, Y.; Paulis, M.; Leiza, J. R. *J. Colloid Interface Sci.* **2010,** *352*, 359–365.

27 Jönsson, J. E. L.; Hassander, H.; Törnell, B. *Macromolecules* **1994,** *27*, 1932–1937.

28 Stubbs, J. M.; Karlsson, O.; Jönsson, J. E.; Sundberg, E.; Durant, Y.; Sundberg, D. *Colloid Surf. A: Phys. Eng. Aspects* **1999,** *153*, 255–270.

29 Lee, C. F. *J. Polym. Sci. Part A: Polym. Chem.* **2005,** *43*, 2224–2236.

30 Tillier, D. L.; Meuldijk, J.; Höhne, G. W. H.; Frederik, P. M.; Regev, O.; Koning, C. O. *Polymer* **2005,** *46*, 7094–7108.

31 Stubbs, J.; Carrier, R.; Sundberg, D. C. *Macromol. React. Eng.* **2008,** *17*, 147–162.

32 Stubbs, J. M.; Sundberg, D. C. *Prog. Org. Coat.* **2008,** *61*, 156–165.

33 Ugelstad, J.; El-Aasser, M. S.; Vanderhoff, J. W. *J. Polym. Sci.: Polym. Lett.* **1973,** *11*, 503–513.

34 Asua, J. *M. Prog. Polym. Sci.* **2002,** *27*, 1283–1346.

35 Manea, M.; Chemtob, A.; Paulis, M.; de la Cal, J. C.; Barandiaran, M. J.; Asua, J. M. *AIChE J.* **2008,** *54*, 289–297.

36 Lopez, A.; Chemtob, A.; Milton, J. L.; Manea, M.; Paulis, M.; Barandiaran, M. J.; Theisinger, S.; Landfester, K.; Hergeth, W. D.; Udagama, R.; McKenna, T.; Simal, F.; Asua, J. M. *Ind. Eng. Chem. Res.* **2008,** *47*, 6289–6297.

37 Alduncin, J. A.; Asua, J. M. *Polymer,* **1994,** *35*, 3758–3765.

38 Chern, C. S.; Poehlein, G. W. *J. Polym. Sci.: Polym. Chem. Ed.* **1987,** *25*, 617–635.

39 de la Cal, J. C.; Urzay, R.Zamora, A.; Forcada, J.; Asua, J. M. *J. Polym. Sci. Part A: Polym. Chem.* **1990,** *28*, 1011–1031.

40 van KrevelenD. W. Properties of Polymers. Their Correlation with Chemical Structure, their Numerical Estimation and Prediction from Additive Group Contributions, 3rd ed.; Elsevier: Amsterdam, **1992,** p 516.

41 Oh, J. K.; Yang, J.; Tomba, J. P.; Rademacher, J.; Farwaha, R.; Winnik, M. A. *Macromolecules* **2003,** *36*, 8836–8845.

42 Wu, J.; Tomba, J. P.; Winnik, M. A.; Farwaha, R.; Rademacher, J. *Macromolecules* **2004,** *37*, 4247–4253.

43 Farinha, J. P. S.; Wu, J.; Winnik, M. A.; Farwaha, R.; Rademacher, J. *Macromolecules* **2005,** *38*, 4393–4402.

44 Tomba, J. P.; Portinha, D.; Schroeder, W. F.; Winnik, M. A.; Lau, W. *Colloid Polym. Sci.* **2009,** *287*, 367–378.

45 Hess, B.; Kutzner, C.; van der Spoel, D.; Lindahl, E. J. *Chem. Theory Comput.* **2008,** *4*, 435–447.

46 Humphrey, W.; Dalke, A.; Schulten, K. J. *Mol. Graph.* **1996,** *14*, 33–38.